Fuel xxx (xxxx) xxx

Contents lists available at ScienceDirect

Fuel

journal homepage: www.elsevier.com/locate/fuel

Full Length Article

Heat release rate shaping for optimal gross indicated efficiency in a heavy-duty RCCI engine fueled with E85 and diesel

Robbert Willems [a,*], Frank Willems [b,c], Niels Deen [a], Bart Somers [a]

[a] Zero-Emission Lab, Eindhoven University of Technology, P.O. Box 513, 5600 MB Eindhoven, The Netherlands
[b] Control Systems Technology, Eindhoven University of Technology, P.O. Box 513, 5600 MB Eindhoven, The Netherlands
[c] TNO Automotive, Automotive Campus 30, 5708 JZ Helmond, The Netherlands

ARTICLE INFO

Keywords:
RCCI
E85
Ethanol
Dual-fuel
Efficiency

ABSTRACT

The understanding of reactivity controlled compression ignition has greatly improved throughout recent years. While its potential for extremely low NO_x and soot emissions has been confirmed numerous times, there remain some ambiguities about the ability of this concept to attain very high efficiency. Now that increasingly stringent CO_2 regulations come into effect worldwide, it is particularly the efficiency aspect that is of great interest. This work combines a heat release study with regression analysis to identify the influence of combustion parameters on the heat release rate shape and the relation it has with efficiency and associated loss channels. A metric called burn ratio is introduced as the ratio of burn durations after and before the centroid of combustion. The burn ratio is found to correlate well to fuel reactivity stratification, and generally characterizes the heat release rate shape. Further regression analysis revealed a synergy between fuel reactivity stratification and the intake manifold pressure. Heavily boosted conditions and relatively early diesel injections result in a notable suppression of heat transfer losses, although some stratification remains necessary to find a balance between heat loss and combustion efficiency. Specifically, this balance is essential to achieve high gross indicated efficiency, for which the burn ratio is finally used to optimize fuel injection.

1. Introduction

The drive for highly efficient and clean engines has moved research towards combustion concepts that provide ample time for mixing of fuel and air prior to ignition. Pioneering work in this field focused on essentially homogeneous, heavily diluted mixtures that are ignited by compression; a process known as homogeneous charge compression ignition (HCCI). These efforts opened up possibilities to achieve very low emissions of nitrogen oxides (NO_x) and soot, while retaining typical diesel engine efficiency. HCCI is governed by chemical kinetics and, hence, it suffers a lack of mixing-controlled combustion phasing that is common for conventional diesel combustion (CDC). To prevent premature ignition and violent combustion, considerable rates of exhaust gas recirculation (EGR) are used to lower the charge reactivity. Boosted intake manifold pressures may also be employed to temper heat release rates, but the auto-ignition tendency possibly increases depending on the applied fuel. These measures endow HCCI with a limited operable load range, also related to mechanical constraints, and high emissions of carbon monoxide (CO) and unburned hydrocarbons (UHC). Moreover, intake manifold pressure and EGR rate settings do not provide the timely response needed for transient engine operation. Various strategies have been proposed to deal with these issues, such as partial stratification of local air-excess ratios (λ) and tailoring of physicochemical fuel properties. Comprehensive overviews of such advanced HCCI engine operating strategies are given by Yao [1] and Saxena [2].

The idea of using two fuels of different reactivities to control ignition and combustion was first introduced by Inagaki et al. [3]. Fuel reactivity is blended to appropriate levels by port fuel injection (PFI) of a low reactivity fuel and direct injection (DI) of a high reactivity fuel. Timing of one or more DI events, scheduled well before the start of combustion (SOC), is used to create varying degrees of reactivity stratification allowing to tune the rate of heat release. The high reactivity fuel initiates combustion by low temperature reactions, producing enough heat and radical species to ignite the rest of the charge. This combustion concept was eventually termed reactivity controlled compression ignition (RCCI) and has been further developed in the last decade by various research groups [4,5].

Conventional gasoline and diesel were initially applied in RCCI

* Corresponding author.
E-mail address: r.c.willems@tue.nl (R. Willems).

https://doi.org/10.1016/j.fuel.2020.119656
Received 15 June 2020; Received in revised form 24 September 2020; Accepted 30 October 2020

combustion, because their wide availability made them interesting fuel candidates. Researchers at the University of Wisconsin-Madison reported an extremely high peak gross indicated efficiency (GIE) of 56% at a moderate load [6], while emitting very low levels of engine-out NO_x and soot. It was furthermore demonstrated that this fuel combination works well over a reasonable range of gross indicated mean effective pressures (IMEP) from about 5 to 15 bar. Still, the intake valve closing (IVC) event had to be retarded at elevated loads to aid in combustion phasing control. Several other studies confirmed the NO_x and soot reduction capabilities of gasoline-diesel RCCI combustion [7–10], but GIE values above 55% were not reproduced. Reasons for that offset may be sought in differences between light and heavy-duty engines [11] and base performance of an engine in CDC mode [12].

Control of CA50 using the diesel injection timing and gasoline percentage has been demonstrated to work acceptably up to moderate loads [13,14]. Other means are necessary to maintain RCCI operation at higher loads [15], because gasoline reactivity proved to be insufficiently low for proper combustion phasing using merely fueling parameters. Strategies that involve lowering the effective compression ratio by IVC adjustments were shown to be adequate in extending ignition delays at elevated loads [16,17]. This can be achieved by either installing an advanced variable valve actuation (VVA) system or changing the cam shaft entirely. This last option poses a tradeoff between low load combustion efficiency and high load operating limits. A pathway to extend the load range with apparently fewer compromises is applying a lower reactivity PFI fuel, as combustion can expectedly be optimized without engine hardware modifications.

Several studies have investigated higher RON fuels for application in RCCI combustion. At least two of such fuels already have a production and retail infrastructure in place: natural gas and E85 (i.e. a blend of 85% ethanol and 15% gasoline by volume). Both of these fuel candidates are expected to play a significant role in the future utilization of alternative fuels [18], both in existing and advanced engine concepts. Natural gas has been successfully applied as low reactivity fuel in heavy-duty RCCI operation [19,20]. In these studies, EGR was shown to be redundant for controlling CA50 from low up to relatively high loads of 17 bar gross IMEP. This feature holds promise regarding brake thermal efficiency (BTE), because of a potentially higher in-cylinder ratio of specific heat capacities and lower pumping losses. Increasing BTE obviously aids the efforts to reduce CO_2, which is further facilitated by the favorable carbon to hydrogen ratio of methane. Unfortunately, the use of natural gas also brings about issues of CH_4 emissions, which have a significantly higher global warming potential and are extremely difficult to reduce using an oxidation catalyst. The latter especially holds at low loads, where exhaust gas temperature is low and the demand for reduction is high.

E85 received considerable attention in research on RCCI, which has shown some favorable aspects. Splitter et al. [21] reported a peak GIE of 59% using PFI of E85 and DI of diesel, while the achievable maximum load was readily extended compared to their work with gasoline. In addition, lower EGR rates were required at all tested load points up to 16.5 bar gross IMEP, while NO_x emissions still remained well within legislative limits. The GIE was enhanced even further to values near 60% using a compression ratio of 18.7 and disabling the piston cooling [22]. The load expansion capabilities of E85 were corroborated by Curran et al. [23] by running tests on the light-duty federal test procedure. Still, concerns were raised on the comparatively low exhaust gas temperatures in RCCI operation that may pose aftertreatment issues and restrict turbocharger capacity. Aside from a load range extension, Benajes et al. [24] also reported an improved CA50 control degree on DI timing by utilizing E85, ascribed to both a higher RON and latent heat of vaporization compared to gasoline. With respect to natural gas, E85 has the additional benefit of being liquid at atmospheric conditions, which alleviates storage and handling procedures. Its main component, ethanol, can furthermore be produced from a wide variety of sustainable resources and considerable progress is made in associated production methods [25].

Despite significant progress developing and understanding RCCI combustion on a laboratory level, the concept has not been put into production to date. With the introduction of CO_2 regulations for heavy-duty vehicles in essentially all major markets [26], and further restrictions to NO_x and soot emissions, the need for highly efficient and clean production engines is evident. Fuel production gradually shifts from fossil sources to renewables, and hence a prerequisite of future heavy-duty engines is a fuel flexible character. This enables running on sustainable fuels from different sources that may strongly vary in composition. RCCI has the potential to fulfill these criteria, but current CO_2 legislation focuses solely on tailpipe emissions, thereby ignoring the carbon footprint reduction from well-to-tank. Current efforts are therefore mainly directed towards optimization of BTE, and the use of ”practical” fuels is favored. The latter are fuel candidates that are compatible with current engine hardware and have the necessary infrastructure ready for swift implementation into the market. The use of E85 in an RCCI engine is thus a promising pathway to meet upcoming regulations within the next decade, but its peak efficiency potential needs to be further investigated to make the concept attractive for development towards production. Not in the least because CDC remains a very competitive technology; development is en route to 55% BTE using a combination of waste heat recovery and incremental combustion system improvements [27].

There are two main objectives set for the current study. First, rates of heat release (ROHR), and integral metrics derived thereof, are analyzed to increase the understanding of heat release behavior under various operational conditions. The goal is to relate key combustion characteristics to engine efficiency and related energy loss channels. Second, this work aims to optimize GIE through dedicated experiments on a single-cylinder engine setup using E85 and diesel as low and high reactivity fuels, respectively. Both fuel injection and air path settings are varied in the tests, and use is made of the Design-of-Experiments methodology. In the following, the experimental setup and methods are first treated, after which the results are presented and discussed. This paper concludes by summarizing the main outcomes and providing an outlook for future work.

2. Experiment

2.1. Engine setup

Experiments are conducted on a single-cylinder test engine adapted from a production variant 12.6 liter DAF XEC. A schematic overview of the setup is shown in Fig. 1, whereas engine and fuel specifications are given in Table 1. Three out of six cylinders run on the standard engine control unit to drive the crank shaft, while two cylinders are entirely non-firing. A Schenck W450 eddy-current brake is used to set and maintain stable engine speeds. The dedicated test cylinder is, except from the crank and cam shafts, completely isolated from the rest of the engine. It has its own air path and fuel systems allowing to freely select operating parameter settings. A common rail system with a Delphi DFI21 injector and double-step piston are installed to match EURO VI specifications. Note that this piston bowl is not optimized for RCCI operation. The compression ratio, on the other hand, has been lowered to 15.85 to prevent excessive peak firing pressures.

Diesel is delivered to the common rail by an air-driven Resato HPU200-625–2 pump. Fuel pressure is measured downstream of the high pressure pump and a feedback controller maintains the desired setting. For PFI of E85, a Bosch EV1 injector is fitted in one of the intake runners of the isolated cylinder, which is in turn driven by a MoTec M400 control unit. E85 is fed to the injector by a low pressure pump located in the fuel tank, which is manually set to approximately 5 bar by adjusting its rotational speed. The applied E85 is in–house blended using anhydrous ethanol and EN228 specification RON95 gasoline at an 85 to 15 volume-based percentage. Fuel consumption of diesel and E85 is

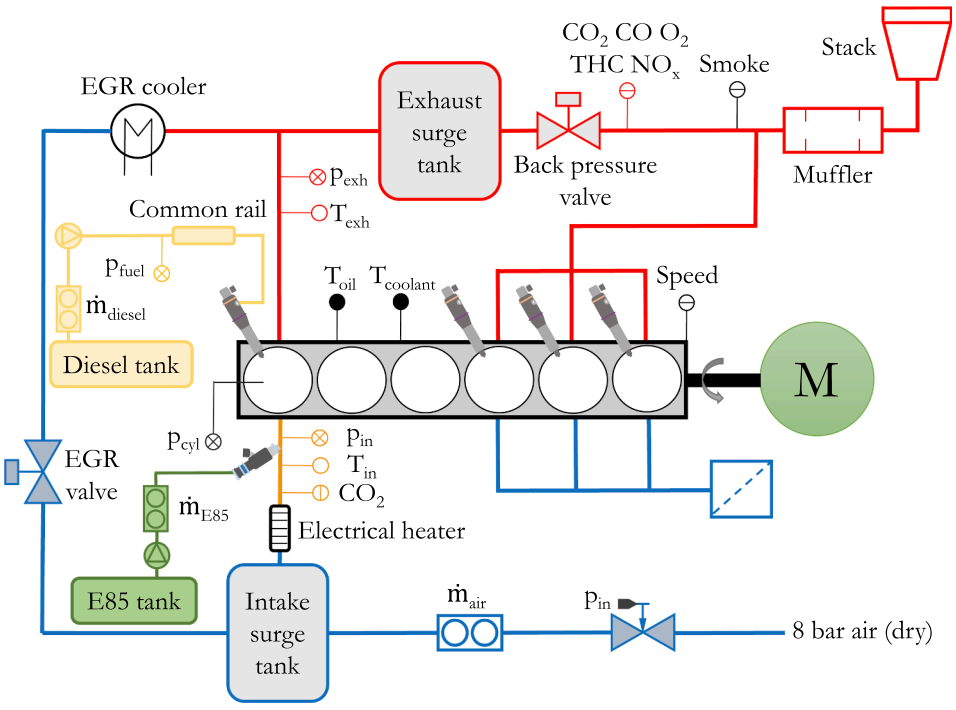

Fig. 1. Schematic of the single-cylinder test setup indicating hot (red) and cold (blue) flows. (For interpretation of the references to colour in this figure legend, the reader is referred to the web version of this article.)

Table 1
Engine and fuel specifications.

Displaced volume	2097 cc
Bore	130 mm
Stroke	158 mm
Compression ratio	15.85
Piston bowl shape	Double-step
Number of valves	4
Exhaust valve closure	-346 CAD aTDC
Intake valve closure	-153 CAD aTDC
Exhaust valve opening	128 CAD aTDC
Intake valve opening	344 CAD aTDC
Diesel injector	Delphi DFI21
Spray included angle	139°
Number of holes	7
Hole size	0.195 mm
Port fuel injector	Bosch EV1
Diesel specifications	EN590 (42.6 MJ/kg)
PFI fuel	E85 (29.1 MJ/kg)

measured using two identical Micro Motion CMF010M mass flow sensors. Gaseous emissions are analyzed using a Horiba MEXA 7100 DEGR system.

Boosted dry air is provided by an external compressor and the intake manifold pressure is adjusted using a regulator. Mass flow of fresh air is subsequently measured by a Micro Motion CMF200M. An electrical heater element is used to maintain a constant intake manifold temperature of 40 °C. Steady pressures and temperatures are furthermore measured at both the intake and exhaust. A back pressure valve is fitted in the exhaust to mimic a variable geometry turbocharger and generate a flow in the high-pressure EGR system. The EGR valve subsequently sets the EGR rate, which is defined as

$$EGR\% = \frac{CO_{2,in}}{CO_{2,exh}} \times 100\%. \quad (1)$$

Recirculated exhaust gas is heavily cooled to approximately room temperature by a cold stream of process water that is connected to a production type EGR cooler. Condensate from the exhaust stream is collected in a vessel and drained in between experimental runs. Surge tanks in both the intake and exhaust paths dampen pressure fluctuations induced by single-cylinder operation. The engine is warmed up to steady oil and coolant temperatures of 90 and 85 °C, respectively, prior to the experiments.

2.2. Signal processing

In-cylinder pressure is measured using an uncooled AVL GU21C piezoelectric transducer wired to a Kistler 5011B charge amplifier. Crank angle information at 0.1 degree resolution is provided by a Heidenhain ROD 420 3600 encoder. These data are logged on a Smetec COMBI data acquisition system, which logs 70 consecutive raw pressure traces for post-processing. These traces are averaged and smoothened with a first-order Savitzky-Golay filter using a sample size of 11 data points. Steady pressures, temperatures, mass flows and species concentrations in intake and exhaust are logged on an in–house built data acquisition system which collects signals at a 20 Hz frequency over a 40 s interval. Mean values are logged for further analysis.

3. Methodology

3.1. Stationary operating conditions

Tests are performed at a single, relatively low load point at approximately 30% of the rated torque at 1200 rpm. The arrangement of the engine setup does not allow for crank shaft torque measurements representative for the test cylinder alone, hence the total fuel energy input is kept constant instead. Gross IMEP thus varies with efficiency between experimental runs of different settings. The nominal stationary settings are summarized in Table 2.

The load-speed point under investigation in this work has been selected for three main reasons. First, this load practically corresponds to highway cruising conditions on a flat road for a loaded heavy-duty truck used for transport. The actual engine torque demand of course depends on total payload, transmission specifications and particular vehicle drag coefficients, but the gross IMEP selected here is regarded

Table 2
Nominal stationary operating conditions.

Gross IMEP	8.5 ± 1 bar
Fuel energy input	3850 ± 100 J/cycle
Engine speed	1200 rpm
P_{exh}-P_{in}	0.3 bar
T_{in}	40 °C
$T_{coolant}$	85 °C
T_{oil}	90 °C

highly common and contributes considerably to the total fuel consumption in routine operation. Second, the aforementioned ⩾55% GIE values in literature were obtained at similar load settings as the one selected in this work, which makes it an interesting target for further research. Third, recent studies have opted for mode-switching to achieve maximum BTE over the full operating map, although approaches differ between publications [28,29]. These studies show that CDC can be used at low loads, as to prevent extreme combustion losses. At high loads, CDC may again be employed, or a switch to conventional dual fuel operation (i.e., with a diesel pilot close to TDC) can be done. The mid load range, as targeted in this work, proved to be most viable for optimal RCCI operation.

3.2. Design-of-experiments

The Design-of-Experiments (DOE) methodology is applied in the engine tests. This approach allows to test several input parameter settings and investigate their interactions without needing to measure all possible combinations. A limited number of publications on the use of DOE in engine research can be found, and its application to RCCI is occasional. In [30], for example, a fractional factorial design is used for conducting simulations to optimize fueling strategies in a natural gas and diesel fueled RCCI engine. In the current work, a central composite design (CCD) is used following the theory of Box and Wilson [31]. This design is useful for detecting curvature in a response, e.g. GIE, and creating response surface plots from regression polynomials. These response surfaces can be used to find operating parameter settings that optimize GIE.

Table 3 displays the fueling and air path parameters (factors) and their settings considered in the CCD experiments. The PFI rate of E85 is expressed as a weight percentage of the total fuel mass. A single DI strategy is applied in this work, where SOA refers to the start of actuation of the solenoid diesel injector. Intake manifold pressure is given in absolute values and the EGR rate is computed according to Eq. 1. It is common practice in DOE to design a test matrix using coded values, which are shown in the upper row of Table 3. These coded values are eventually converted to physical values, but the relative distances remain the same. The base of a CCD is a two-level full factorial design, meaning that all combinations between the factors at two levels (-1 and 1) are run. The CCD is then complemented by a unique center point (0) that is repeated at several random instances to assess repeatability and drift. The mean GIE at the center point was determined to be 47.5% with a standard deviation of 0.3%. Axial points are lastly added to finalize the matrix, in which one of the factors is set to an extremum while the others are set to their center point value. The resulting number of experimental runs equals $2^k + 2k + C$, where k is the number of factors and C is the number of center point measurements. For Table 3, k and C both equal 4, and the entire set was run twice, amounting to 56 runs in total. The coded values of the axial points (α) are determined using

$$\pm\alpha = \sqrt[4]{2^k}. \tag{2}$$

For $k = 4$, the coded values amount to −2 and 2.

Table 3
Factors and levels used in the CCD experiments.

Factor	$-\alpha$	−1	0	1	α
PFI rate (E85) [wt%]	65	70	75	80	85
SOA (diesel) [CAD aTDC]	−57.5	−50	−42.5	−35	−27.5
Intake manifold pressure [bar(a)]	1.6	1.8	2.0	2.2	2.4
EGR rate [%]	0	5	10	15	20

3.3. Regression procedure

For further response surface analysis, regression polynomials are fitted to the experimental data resulting from the CCD matrix. A response variable ϕ is represented by a regression equation of the form

$$\phi = \beta_0 + \beta_1 x_1 + \beta_2 x_2 + \beta_3 x_1 x_2 + \beta_4 x_1^2 + \beta_5 x_2^2. \tag{3}$$

Here, ϕ is presented as a two-factor example that estimates the response at any point (x_1, x_2) in the factor space. Ordinary least squares fitting is applied with a forward selection scheme (i.e., a stepwise procedure in which terms are added one by one) to find the best fit. This scheme determines the eventual number of terms for a particular regression equation. Single factor terms, two-factor interaction terms and quadratic terms are each tested for significance using p-values ascribed to individual terms. A p-value below 0.05 is considered significant in this work. To further support the claim of significance, terms are only added when they contribute to an increase in the adjusted R^2 value of the resulting model. This adjusted R^2 accounts for the number of terms in relation to the number of data points, as to prevent overfitting. An overview of the three regression models that will be used in the analysis is given in Table 4. Accuracy of these models is checked by plotting residuals ($\phi_{exp} - \phi$) as function of the predicted values to ascertain that a proper polynomial degree is applied. Residuals are also plotted versus the measurement number in chronological order to detect potential experimental drift. A second set of experiments consisting of SOA sweeps was run to optimize GIE and supplement more insight on relevant processes and metrics. The results of these SOA sweeps will be discussed in Section 4.5.

3.4. Energy fractions

Fuel energy distributions are computed to quantify individual loss channels and pinpoint directions for further GIE optimization. GIE is expressed by

$$GIE = \frac{\oint_{\theta=-180}^{\theta=180} p \, dV}{m_f \, LHV_f}, \tag{4}$$

where θ is the crank angle, p is the instantaneous pressure, V is the combustion chamber volume, m_f is the sum of the E85 and diesel masses. LHV_f is the lower heating value of the fuel blend based on the current PFI to DI balance determined via

$$LHV_f = \frac{\dot{m}_{PFI} LHV_{PFI} + \dot{m}_{DI} LHV_{DI}}{\dot{m}_{PFI} + \dot{m}_{DI}}, \tag{5}$$

Table 4
Overview of R^2_{adj} values and prediction terms included in the models.

Model	R^2_{adj}	Main terms	Cross terms	Quadratic terms
Heat transfer loss	0.939	PFI, SOA, p_{in}	PFI·SOA, SOA·p_{in}	PFI^2, SOA^2, p_{in}^2
Combustion efficiency	0.923	PFI, SOA, p_{in}, EGR	SOA·EGR	PFI^2, SOA^2
Burn ratio	0.977	PFI, SOA, p_{in}	PFI·SOA, SOA·p_{in}	SOA^2

where $\dot{m}_{PFI}$ and $\dot{m}_{DI}$ are the mass flows of E85 and diesel, respectively.

The combustion losses (CL) due to incomplete conversion of fuel to CO_2 and water are inferred from the emissions of CO and HC. It is expressed by

$$CL = \frac{ISCO\ LHV_{CO} + ISHC\ LHV_f}{ISFC\ LHV_f}, \tag{6}$$

where *ISCO* and *ISHC* are the gross indicated specific emissions of CO and HC, respectively, and *ISFC* is the gross indicated specific fuel consumption. LHV_{CO} is the lower heating value of CO. The *LHV* of HC is assumed to be identical to that of the fuel blend (LHV_f), equal to the approach of Pedrozo et al. [32]. Flame ionization detectors (FID) are less sensitive to oxygenated compounds in the exhaust sample [33]. The HC readings are therefore corrected for the use of ethanol using the correlation provided by Kar and Cheng [34].

Determining the in-cylinder heat losses is generally difficult. The total amount of heat transfer to the surfaces of the piston, liner and cylinder head is often used as a closing term after calculation of the previously defined efficiencies and the sensible heat in the exhaust stream. Thermocouples can in principle be used to determine the latter, but typical temperature measurements are done somewhere downstream of the cylinder head. While this does provide insight in the amount of sensible heat that can be used to drive a turbine or light-off a catalyst, the residual energy cannot simply be ascribed to in-cylinder heat transfer, as additional heat is lost to exhaust valves, cylinder head and the exhaust manifold. Another prevailing method is the use of empirical correlations. An adapted version of the original Woschni model has been suggested by Chang et al. [35] for premixed combustion concepts. However, as with the original model, certain constants need to be tuned for different engines and operating conditions. This limits the usefulness of such correlations and leads to uncertainties that are difficult to eliminate.

In this work, heat release information derived from the pressure trace is used to assess the total heat transfer to combustion chamber surfaces. The apparent rate of heat release (aROHR) is determined via the first law of thermodynamics and is expressed by

$$\frac{dQ}{d\theta} = \frac{\gamma}{\gamma - 1}\ p\ \frac{dV}{d\theta} + \frac{1}{\gamma - 1}\ V\ \frac{dp}{d\theta}, \tag{7}$$

where γ is the temperature and composition dependent specific heat capacity ratio, which is determined using the NASA polynomials, the global gas temperature and average gas composition at θ. The gas compositions in the intake and exhaust are determined using gas analyzer data, which are taken as unburned and burned fractions, respectively, and are assumed to transition linearly during combustion. The main uncertainties in this approach come from the heat release calculation, which needs careful consideration. The combustion chamber volume (V) is computed with a model using the geometric specifications shown in Table 1, which were acquired from the manufacturer. Analyzing the gas composition and measuring the cylinder pressure may introduce slight errors, which were minimized by regular calibration of sensors and detectors. The aROHR is finally integrated over all crank angles from IVC to exhaust valve opening (EVO). By evaluating the energy state upon EVO and subtracting this value from the total energy released by combustion, the integrated heat loss is obtained. The method is graphically exemplified in Fig. 2.

The fraction of heat transfer loss (HL) to the total fuel energy input is expressed by

$$HL = \frac{Q_{ht}}{m_f\ LHV_f}. \tag{8}$$

And finally, the energy that is expelled via the exhaust is taken as the residual energy to close the energy balance via

$$EL = 1 - CL - HL - GIE. \tag{9}$$

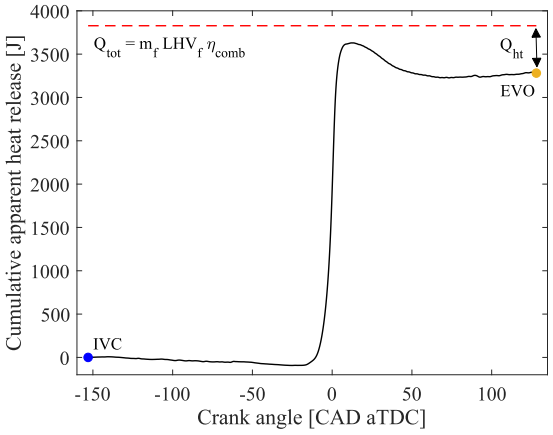

Fig. 2. Cumulative apparent heat release as function of crank angle in a typical experiment.

Note that this quantity does not necessarily yield the useable energy in the exhaust stream. Some of the energy may still end up in the cooling circuit by heat transfer to the exhaust valve or port.

4. Results and discussion

Increased interest in RCCI in recent years stems from its potential to attain high thermal efficiency at extremely low engine-out NO_x. To fully utilize these capabilities, a solid understanding of the combustion process is required. RCCI combustion is governed by chemical kinetics, the rate of which is predominantly dependent on how the combustible charge is prepared. This, in turn, relies on the fuel injection and air path settings. In the following, rate of heat release traces are analyzed, from which a combustion metric is derived called the burn ratio. It is demonstrated that this burn ratio relates to the rate of heat release shape, fuel reactivity stratification and GIE. Thereafter, a regression analysis is done to assess how heat transfer and combustion losses can be best balanced to optimize the GIE. It is shown how this is established using the available operational parameters in Table 3. Finally, additional sweeps of SOA are presented to optimize GIE, and use of the burn ratio is proposed as an optimization guideline.

4.1. Impact of reactivity stratification on the rate of heat release

Mixture preparation is of utmost importance for the chemical kinetics and thermodynamic processes within the combustion chamber. This is discussed by Splitter et al. [36], who have used two distinctive equivalence ratios to describe the degree of fuel reactivity stratification and global charge dilution. The premixed equivalence ratio ($\Phi_{premixed}$), i.e., that of the charge prepared in the intake manifold, was used to specify the fuel reactivity stratification at a constant diesel injection timing. The global equivalence ratio (Φ_{global}), i.e., that of charge in the cylinder when the low and high reactivity fuels are mixed together, described the total charge dilution. It was found that lean global operation can increase GIE through reductions of heat transfer, but that stratification is necessary to find the best tradeoff between heat transfer and combustion losses. While $\Phi_{premixed}$ at a given Φ_{global} certainly is a measure for the reactivity span in the combustion chamber, it does not consider the time available for mixing of high reactivity fuel after injecting it directly into the cylinder. This does, however, influence the local diesel concentration to a large extent [37]. In this work, the diesel injection timing is indeed varied and, thus, a measure of available mixing time is needed. The ignition dwell (*IDw*) is expressed by

$$IDw = CA10 - EOI, \tag{10}$$

where *EOI* is the end of the direct injection event and *CA*10 is the crank

angle at which 10% of the total heat is released, here taken as the start of combustion. The value of *IDw* is directly affected by the diesel injection timing via *EOI*, but also by the PFI rate, intake manifold pressure and EGR rate through changes in *CA*10.

Experiments were run according to the matrix in Table 3 and as described in Section 3.2. Subsequent aROHR analysis revealed vastly different rate shapes under varying operational settings, which was then further investigated. It was observed that the aROHR can exhibit either a single-stage or dual-stage heat release rate, depending on the specific level of fuel reactivity stratification. A combustion metric called the burn ratio was defined that characterizes this feature, which is the ratio of the phase-specific burn durations after and before CA50,

$$R_b = \frac{CA90 - CA50}{CA50 - CA10}. \tag{11}$$

Fig. 3 shows various aROHR traces for an ensemble of R_b values taken from the data set, where a decreasing value of R_b marks the transition from dual-stage heat release rates towards a single stage. Note that the x-axis should not be interpreted as the crank angle domain, but rather allows for a side-by-side comparison of rate traces. For extremely high levels of fuel reactivity stratification, diesel fuel is locally concentrated, thereby creating regions of substantial reactivity. These regions will ignite first and burn rapidly, owing to the relatively fuel rich conditions and strong autoignition tendency of diesel. As a consequence, these heavily stratified conditions correlate to excessively advanced combustion, i.e., CA50 values well before TDC. Kokjohn, Musculus and Reitz [38] studied these ignition mechanisms through a combination of high-speed chemiluminescence imaging and modeling of chemical kinetics. They found that combustion starts in the squish region, and that the ignition delay gets progressively longer towards the combustion chamber center, thereby mainly following gradients in the concentration of the high reactivity fuel. Therefore, it is expected that under circumstances of considerable stratification, those regions with a low diesel concentration will burn late and slow. The dual-stage heat release rate seen in Fig. 3 for $R_b > 1$ is ascribed to this mechanism. As the diesel is given more time to mix with the already present premixed charge, the degree of fuel reactivity stratification goes down and the initial stage intensity decreases. Combustion phasing is concurrently retarded. Eventually, the aROHR shape develops into a single-stage heat release rate for moderate to low stratification levels. The single aROHR peak rises and the charge burns out faster, as mixing time is increased and lower values of R_b are attained. On the other hand, the first stage of combustion is seen to progress relatively slow for these well mixed cases, which may in part be attributed to specific chemical properties of ethanol. Sjöberg and Dec [39] found that in HCCI combustion, ethanol shows very little low and intermediate temperature heat release. Temperature rise rates are hence only moderate until high temperature heat release commences. While experimental conditions in this work are different, it is probable that this plays a role in the first phase of combustion, given the large amount of ethanol present.

The preceding discussion emphasized the impact of the diesel mixing time (*IDw*) on stratification. The fuel injection parameters take on the most important role in controlling *IDw*, which are the DI SOA (diesel) and the PFI rate (E85). These parameters will be used later on to control R_b and optimize GIE. Note that local temperature also affects ignitability. Even if temperature stratification is negligible at IVC, wall heat transfer and fuel evaporation can induce temperature changes later in the compression stroke [40]. Yet, this is generally not considered a controllable process and will be excluded from this discussion.

Fig. 4 shows a scatter plot of *IDw* and GIE as function of R_b for all DOE runs, thus including variations in all four operating parameters. It can be seen that a clear relation exists between the burn ratio and the ignition dwell. An exponential description appears quite suitable, which follows a general description for convective-diffusive mixing in a turbulent jet. This is further corroborated by the exponential fit and R^2 value. However, there are limitations to that description since the injection duration is only short and transient jet characteristics come into play after injection. Jet velocity along the center axis does not remain constant. Musculus and Kattke [41] studied the mixing behavior of diesel and air after the EOI by transient jet modeling. They found that mixing rates in the wake of the injection pulse momentarily increase just after EOI, due to an entrainment wave that quickly travels upstream and thereby speeds up mixing along the center axis of the entire jet. This could lead to longer *IDw* than expected from the exponential fit especially for large R_b values. For larger values of *IDw*, and thus lower values of R_b, an increasing amount of momentum has been exchanged between the

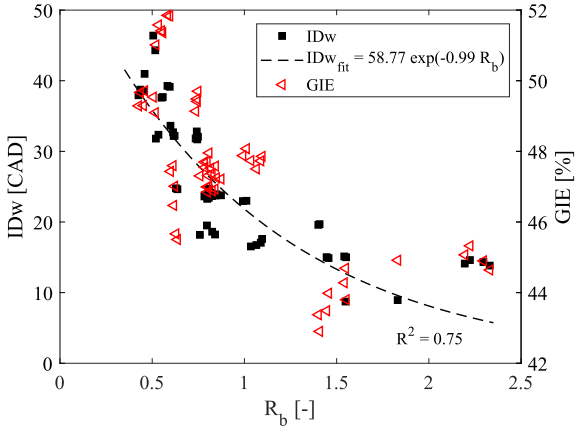

Fig. 4. The ignition dwell (*IDw*) and gross indicated efficiency (GIE) versus the burn ratio (R_b) for all measured DOE points.

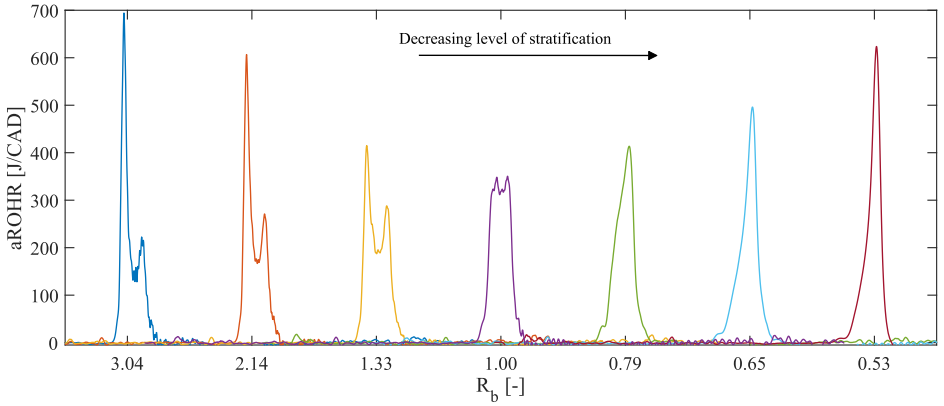

Fig. 3. Rates of heat release (aROHR) for various burn ratios (R_b).

diesel jet and rest of the charge, which slows the mixing rate over time. The fit may be improved by incorporating these mechanisms, but this is out of the scope of this work.

GIE is also plotted in Fig. 4, which displays an upward trend with decreasing R_b, showing the importance of fuel reactivity stratification. Using R_b as an indicator, it is clear that low levels of stratification, i.e., low R_b, result in high efficiency. But despite this clear trend, quite some spread in these GIE data remains. This is an indication that not only fuel reactivity stratification plays a role, but that some of the variance is explained by other quantities. In the next section, a regression analysis is performed to identify important operating parameters and their interactions, relevant for maximizing GIE. It is discussed how these parameters relate to associated energy loss channels through fuel reactivity stratification and other potential governing mechanisms.

4.2. Identifying important parameters for efficiency optimization

A four-way analysis of variance (ANOVA) is first performed on the GIE data to discern important factors and interactions [42]. The resulting ANOVA table is depicted in Table 5, where a double horizontal line separates statistically significant terms from the rest. The first column shows the factors and interactions that are tested and also includes an entry for the experimental error (i.e., variation that is not due to any of the tabulated factors and interactions) and total variation in the data. The second column depicts the sum of squares (SS) for each source. Mean squared (MS) values in the fourth column are computed by dividing SS by the degrees of freedom (d.f.) in the third column. F-values in the fifth column are calculated as the ratio of each MS values and the mean squared error, and finally, an F-test is performed at a 95% confidence level of which the resulting p-values are shown in the rightmost column. The results in Table 5 evidence that three factors have a strong impact on GIE, namely SOA, the PFI rate and the intake manifold pressure. Furthermore, the interaction of the two fueling parameters, as well as the interplay between intake manifold pressure and SOA, prove to be significant.

The impact of fuel reactivity stratification on GIE was discussed in Section 4.1 and the importance is again stressed by the ANOVA results: both fueling parameters affect GIE to a large extent. Hereafter, it is investigated how fuel injection settings influence separate energy loss channels, through response surface analysis. RCCI is often linked to lower heat transfer losses as compared to CDC [43], but on the other hand suffers from higher combustion losses, especially at low loads. Hence, attention is directed to optimizing those particular loss channels using fueling parameter settings, and their relation to the formerly introduced burn ratio. Thereafter, a similar approach is used to study the effects of intake manifold pressure and SOA on these energy loss channels. The ANOVA table implies that this, too, is an important interaction effect and thus deserves further investigation. EGR is interestingly seen to be of insignificant influence on GIE with respect to the other factors.

Table 5
Four-way ANOVA table of GIE data.

Source	SS	d.f.	MS	F	p
SOA	98.84	1	98.84	1294.97	2.34e−20
PFI	54.19	1	54.19	709.98	1.13e−17
pIntake	19.25	1	19.25	252.19	3.56e−13
SOA·pIntake	3.52	1	3.52	46.12	1.02e−6
PFI·SOA	0.87	1	0.87	11.41	2.80e−3
EGR	0.27	1	0.27	3.53	0.07
PFI·pIntake	0.18	1	0.18	2.37	0.14
pIntake·EGR	0.17	1	0.17	2.19	0.15
SOA·EGR	0.02	1	0.02	0.23	0.64
PFI·EGR	0.02	1	0.02	0.20	0.66
Error	1.60	21	0.08		
Total	178.92	31			

Generally, EGR is applied to lower the charge reactivity as a means to control combustion phasing. Although it is thought that this effect is present, it is here only minor due to the relatively low EGR rates applied in the experiments.

4.3. Effects of fuel injection settings

Fig. 5 shows a response surface plot of R_b as function of SOA and the E85 weight percentage. The intake manifold pressure is set to 2 bar in this plot, whereas the EGR rate has been entirely excluded from the regression polynomial due to a statistically insignificant effect. The largest values of R_b are found at the most retarded SOA and lowest E85 percentages, which is in line with the analysis of Section 4.1. This upper left region corresponds to heavily stratified conditions, since *IDw* is in its low range. As the diesel injection is advanced, or the relative amount of E85 is increased, the value of R_b reduces. Furthermore, a combination of the two measures proves most effective in lowering R_b owing to their interaction effect. As a result, the lowest burn ratios are found in the bottom right region of the response surface, where stratification is minimal.

A response surface plot of the heat loss percentage (HL), Eq. (8) is shown in Fig. 6. The selected intake manifold pressure corresponds to Fig. 5. Reducing the degree of fuel reactivity stratification is evidently effective in lowering heat transfer losses, since a directional reduction of R_b correlates to a decline of HL. Two mechanisms are expected to play a role. First, as SOA is advanced the diesel is allowed more time to distribute, which reduces the local ignitability. Combustion phasing is thereby retarded, which has an evident effect on the temperature history. This can similarly be achieved by increasing the E85 percentage. Second, heat loss is governed by local temperatures at the surfaces where heat is actually transferred to the coolant. It thus matters where such high temperatures are reached. This is expected to be near the liner where most of the diesel has been forced to by spray momentum. By alleviating stratification through mixing, these local temperatures will be suppressed.

Fuel reactivity stratification also impacts on the combustion efficiency as can be seen in Fig. 7, which is again plotted using an intake manifold pressure of 2 bar. Particular fuel injection settings provide an optimum of 97.5%. While heavily stratified conditions around an SOA of −30 CAD aTDC lead to the lowest combustion efficiency, the optimum is still located in a slightly more stratified region compared to the optimal setting for the heat transfer loss. And, hence, a tradeoff is clear: preventing high heat transfer losses requires low stratification, while combustion efficiency pushes the optimal fueling settings towards slightly lower E85 percentages and retarded diesel injection timings. Careful calibration will be required to balance this tradeoff.

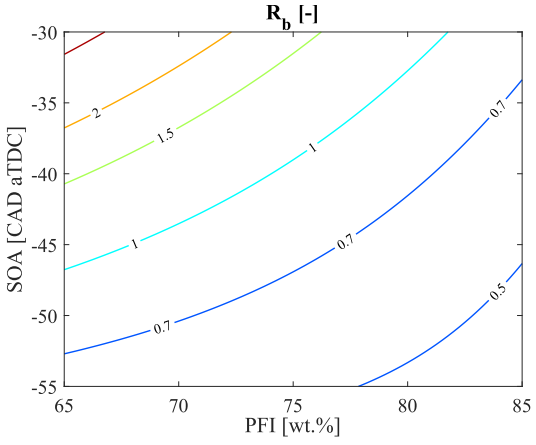

Fig. 5. Prediction of burn ratio (R_b) as function of the PFI rate and DI SOA. The intake manifold pressure is set to 2 bar(a).

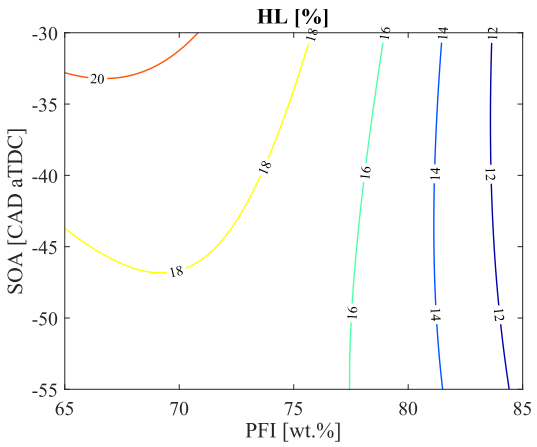

Fig. 6. Prediction of heat loss percentage (HL) as function of the PFI rate and DI SOA. The intake manifold pressure is set to 2 bar(a).

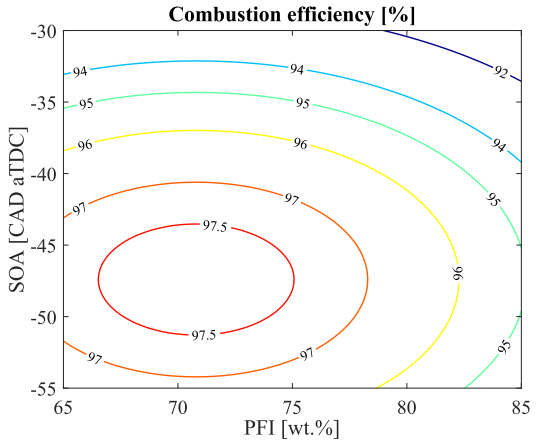

Fig. 7. Prediction of combustion efficiency ($1-CL$) as function of the PFI rate and DI SOA. The intake manifold pressure is set to 2 bar(a).

4.4. Interaction effect of SOA and boost pressure

The ANOVA results in Table 5 show that intake manifold pressure has a strong impact on GIE. Furthermore, the interaction effect of SOA and the intake manifold pressure is also evident. Fig. 8 presents regression curves of the heat loss percentages as function of SOA for three different intake manifold pressures. Shaded regions around the regression curves illustrate a 95% prediction confidence interval. Note that these bounds are affected both by the data sample size and the standard deviation in the sample. In the previous discussion, it became clear that fuel reactivity stratification plays a key role in the total amount of heat loss, and the tradeoff that it displays with combustion efficiency. In Fig. 8, the stratification is controlled only by SOA, since the E85 percentage is kept constant. Splitter et al. [36] found that low values of Φ_{global}, i.e., overall lean conditions, promote high efficiency. That, however, is here seen to only be partly the case. For the most retarded diesel injection timings, elevated boost pressures (low Φ_{global}) tend to exceed the heat transfer loss of lower intake manifold pressures. But as SOA is advanced, the differences between the cases enlarge in favor of heavily boosted conditions, although the effect subsides towards higher boost levels. This behavior exemplifies the strong interaction between SOA and intake manifold pressure, but also points out that there is another characteristic to consider along with stratification. It raises the question: why is heat loss so strongly reduced at elevated boost pressure and advanced diesel injection? To answer that question, the effect of increasing the boost pressure on global temperature needs to be clarified.

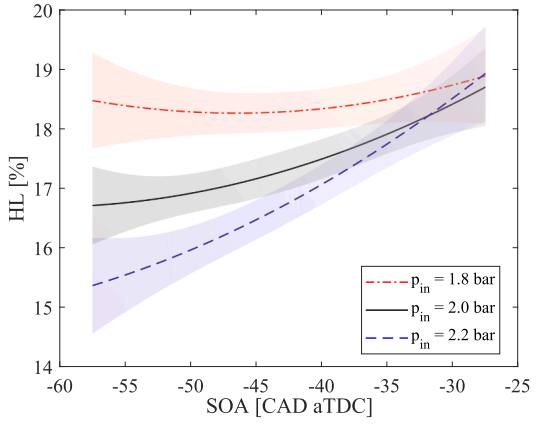

Fig. 8. Prediction of heat loss percentage (HL) as function of DI SOA for three intake manifold pressures. The PFI rate is set to 75 wt%. Shaded regions indicate 95% confidence intervals.

Fig. 9 depicts global gas temperature traces inferred from the cylinder pressure via the ideal gas law for three intake manifold pressure settings. Increasing the intake manifold pressure results in a decrease of peak global gas temperature and in the remainder of the expansion stroke. Still, that does not directly mean that local temperatures are reduced as well, since the latter is coupled to the local equivalence ratio. Here, the degree of stratification again comes into play. Giving the injected diesel more time to blend by advancing SOA creates a more uniform, overall lean charge. Local temperatures then tend to settle towards the global gas temperature, which helps in suppressing heat transfer.

The effect of intake manifold pressure on combustion losses is investigated in Fig. 10, where the combustion efficiency is plotted versus SOA for three boost levels. The curves decrease with each increment of intake manifold pressure mainly due to a lower global temperature. This introduces another tradeoff with the heat transfer losses: boost pressure cannot be increased indefinitely, because of eventual excessive combustion losses. Once again, the need for careful selection of fuel injection and air path settings is clear.

4.5. Optimizing gross indicated efficiency

So far, it has been shown that fuel reactivity stratification plays a key role in finding a good compromise between heat transfer and combustion losses. Rates of heat release were shown to exhibit specific shapes

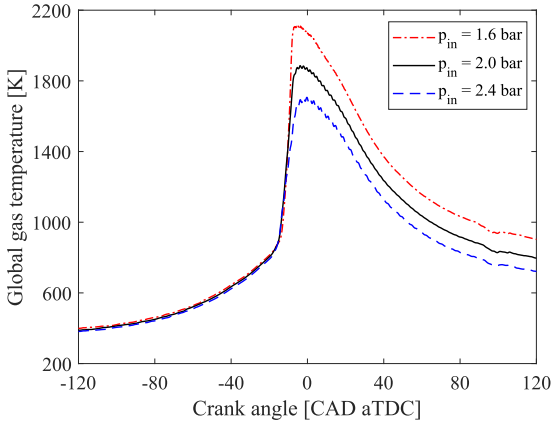

Fig. 9. Global gas temperature versus crank angle for three intake manifold pressures. The SOA is set to −42.5 CAD aTDC, whereas the PFI rate equals 75 wt%.

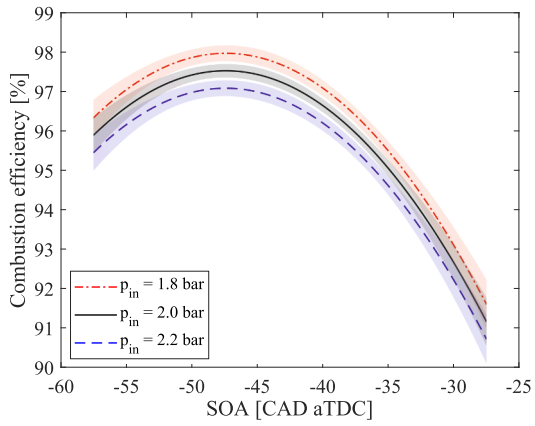

Fig. 10. Combustion efficiency (1 - CL) as function of SOA for three intake manifold pressures. The PFI rate is set to 75 wt%. The shaded regions indicate 95% confidence intervals.

according to the level of stratification, which was analyzed through a combustion metric called burn ratio (R_b). GIE generally increases as the value of R_b goes down, yet, R_b did not quite explain all variation seen in the GIE data. Further regression analysis revealed that stratification and total charge mass - varied through the intake manifold pressure - display a crucial synergy for balancing heat transfer and combustion losses. Particularly low heat transfer losses are found for high boost levels in combination with relatively early SOA settings. In the remainder of this section, SOA sweeps at various percentages of E85 are presented to find maximum GIE at the specific load-speed point under investigation. The intake manifold pressure is set to a relatively high value of 2.4 bar, which was a priori determined to provide the best results. External EGR is entirely omitted, since the ANOVA deemed it statistically insignificant.

In the following, the burn ratio is suggested as a more direct predictor of peak GIE along variations in SOA, instead of the somewhat conventional use of CA50. Fig. 11 depicts CA50 as function of multiple fueling combinations used in these sweeps. Many of the settings result in too advanced combustion phasing, even reaching −10 CAD aTDC. Only the highest two E85 percentages with sufficiently early SOA lead to CA50 values that are near TDC. As can be seen, the SOA advance is not the same for all PFI rates, which was done to prevent misfires. This lack of tolerance to later combustion phasing was previously explained by an absence of low temperature reactions with ethanol combustion [39]. Hence, there appears to be only a small window of suitable CA50 values. Moreover, combustion phasing before TDC is rather counterintuitive when it comes to finding maximum efficiency, as from a CDC standpoint one would expect optimal phasing at several CAD after TDC. Besides, there is no real indication in these CA50 trends that the mixture is tending to misfire, yet it was found in the experiments that there is a very thin line between stable operation and complete misfires.

Fig. 12 shows the SOA sweep results in a NO_x versus CA50 plot. The NO_x emissions are included here because of their significant relevance in engine development. A very strong response to injection timing is seen in these NO_x data, which span a region between levels that comply with EURO VI (0.4 g/kWh) legislation and nearly 20 g/kWh. Combustion phasing again plays a crucial role, as the direction of NO_x increase corresponds to an advance of CA50. The effect of mixing time is also noticeable, since a constant CA50 gives rise to a larger amount of engine-out NO_x at higher E85 percentages. This is caused by the necessity to retard the diesel injection timing when the E85 percentage is increased, thereby leaving less time for mixing. All E85 percentages possess the ability to comply with EURO VI levels from an engine-out perspective, as long as the diesel is allowed sufficient time to mix.

The GIE results are plotted against R_b in Fig. 13; R_b appears to be a good predictor of peak efficiency. For all E85 percentages, GIE is increased as R_b is reduced. At a certain point, the efficiency increase stagnates when the thermal efficiency and combustion efficiency settle in an optimal balance. The reasons for this were outlined in Section 4.2. Fig. 13 indicates that the decrease of R_b also stagnates when GIE peaks. Another look at Fig. 3 is required to understand this behavior. The graph showed that when more time is available for mixing, the first phase of combustion (i.e., denominator of Eq. 11) lengthens, whereas the second phase (numerator), contrarily, progresses faster. When the charge is overly mixed, however, the limit of this fast burnout is reached. The burn ratio decrease hence stagnates, and in some of the presented cases even rises again, which is shown in the zoom view included in Fig. 13 to provide more detail.

The observed stagnation of both the GIE increase and R_b decrease is established when the combustion efficiency deteriorates to the point that potential thermal efficiency benefits (e.g., lower heat losses) cannot compensate this decline. This is shown in Fig. 14 where energy distributions for the 80% E85 case are displayed. In the last step of SOA advance, R_b increases from 0.65 to 0.70, after it was reduced in the first two SOA steps. This R_b increment is accompanied with a notable increase of combustion losses, while heat losses remain nearly constant. The burn ratio, hence, does not only relate to the aROHR shape, it also predicts the position of peak GIE quite well when varying SOA. Compared to previous work by the authors [44] at a similar load setting, the peak GIE of 52.6% in these experiments is higher than for the same engine running in gasoline-diesel RCCI mode (50.9%) or conventional diesel combustion (49.6%).

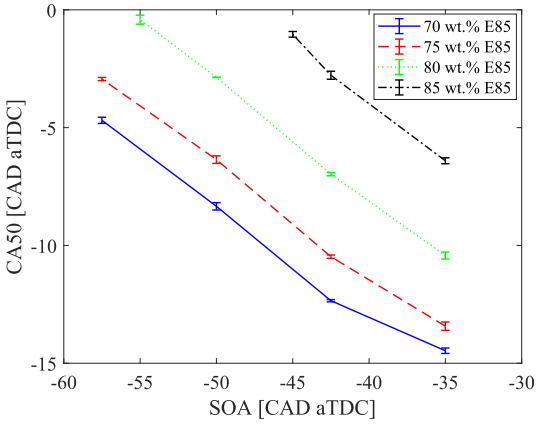

Fig. 11. CA50 for various fueling parameter settings. The error bars show the standard deviation around the mean of three measurements. Further advance of SOA is limited due to the occurrence of misfires.

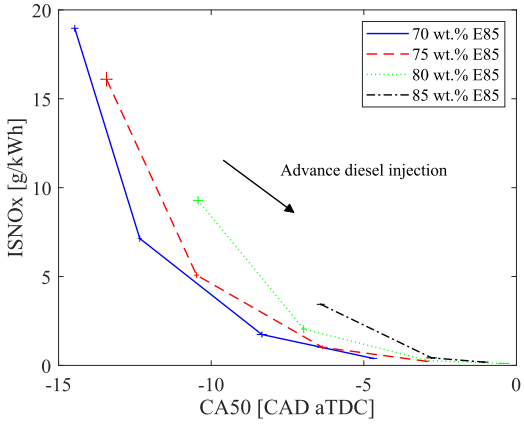

Fig. 12. $ISNO_x$ as function of CA50 for different E85 percentages. The error bars show the standard deviation around the mean of three measurements.

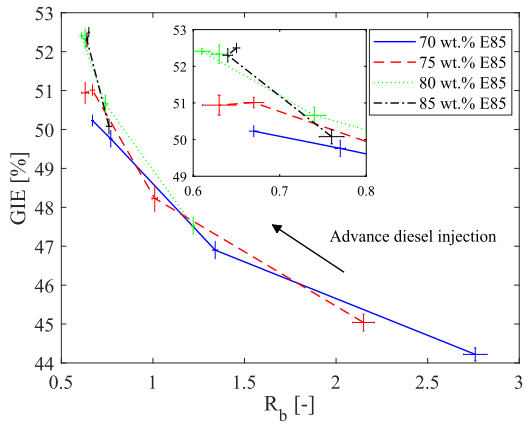

Fig. 13. GIE as function of R_b for different E85 percentages. The error bars show the standard deviation around the mean of three measurements.

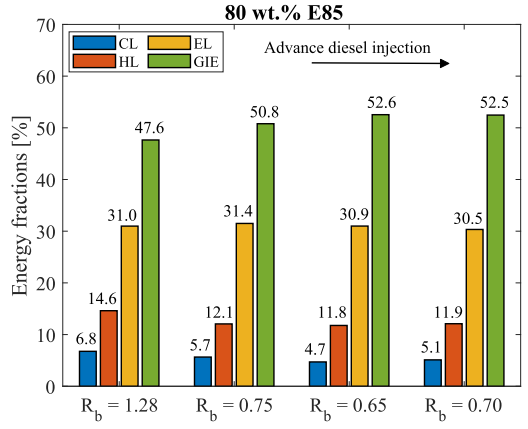

Fig. 14. Energy fractions for various burn ratios (R_b) in an SOA sweep at a PFI rate of 80 wt%.

5. Conclusions and outlook

This work combined a heat release study with regression analysis to shed light on the influence of stratification on the gross indicated efficiency and related energy loss channels in RCCI combustion. The main outcomes of this research are:

- A distinctive combustion metric termed burn ratio is introduced, which correlates well with fuel reactivity stratification, and is shown to characterize the rate of heat release shape.
- The burn ratio is, through fuel reactivity stratification, linked to heat transfer loss and combustion efficiency.
- A strong reduction of heat loss is established through a combination of low fuel reactivity stratification - thus low burn ratio - and high intake manifold pressure, which proved crucial for maximizing the gross indicated efficiency.
- The burn ratio was used to identify the most favorable balance between heat loss and combustion efficiency, making it a practical metric for gross indicated efficiency optimization.

The results presented in this work confirm that E85 is a viable fuel for RCCI operation in heavy-duty engines, allowing peak GIE to be reached at engine-out NO_x levels that comply with current legislation for tailpipe emissions.

How the findings in this work relate to higher loads and speeds is yet unclear and needs to be addressed in future work. For the medium load applied here, the maximum peak pressure and pressure rise rate constraints were not violated. But to attain sufficient charge dilution at higher loads, the intake manifold pressure cannot be increased indefinitely and thus EGR has to be applied. It particularly needs to be investigated whether low burn ratios can be attained at higher loads, and how this relates to emission limits and engine constraints.

CRediT authorship contribution statement

Robbert Willems: Conceptualization, Methodology, Formal analysis, Investigation, Writing - original draft, Visualization. **Frank Willems:** Conceptualization, Formal analysis, Writing - review & editing, Supervision, Project administration, Funding acquisition. **Niels Deen:** Conceptualization, Formal analysis, Writing - review & editing, Supervision. **Bart Somers:** Conceptualization, Formal analysis, Writing - review & editing, Supervision, Project administration, Funding acquisition.

Declaration of Competing Interest

The authors declare that they have no known competing financial interests or personal relationships that could have appeared to influence the work reported in this paper.

Acknowledgments

This work was funded by the Applied and Engineering Sciences (TTW) domain of the Dutch Research Council (NWO) under project number 14927: Towards a HiEff Engine. The authors in particular wish to thank Bogdan Albrecht, Tony Simpson, Erik Doosje and Cemil Bekdemir for valuable discussions and advice.

References

[1] Yao M, Zheng Z, Liu H. Progress and recent trends in homogeneous charge compression ignition (HCCI) engines. Prog Energ Combust Sci 2009;35:398–437. https://doi.org/10.1016/j.pecs.2009.05.001.
[2] Saxena S, Bedoya ID. Fundamental phenomena affecting low temperature combustion and HCCI engines, high load limits and strategies for extending these limits. Prog Energ Combust Sci 2013;39:457–88. https://doi.org/10.1016/j.pecs.2013.05.002.
[3] Inagaki K, Fuyuto T, Nishikawa K, Nakakite K, Sakata I. Dual-fuel PCI combustion controlled by in-cylinder stratification of ignitability. SAE Technical Paper 2006-01-0028. https://doi.org/10.4271/2006-01-0028.
[4] Reitz RD, Duraisamy G. Review of high efficiency and clean reactivity controlled compression ignition (RCCI) combustion in internal combustion engines. Prog Energ Combust Sci 2015;46:12–71. https://doi.org/10.1016/j.pecs.2014.05.003.
[5] Paykani A, Kakaee A, Rahnama P, Reitz RD. Progress and recent trends in reactivity-controlled compression ignition engines. Int J Eng Res 2016;17:481–524. https://doi.org/10.1177/1468087415593013.
[6] Kokjohn SL, Hanson RM, Splitter DA, Reitz RD. Fuel reactivity controlled compression ignition (RCCI): a pathway to controlled high-efficiency clean combustion. Int J Engine Res 2010;12:209–26. https://doi.org/10.1177/1468087411401548.
[7] Curran S, Prikhodko V, Cho K, Sluder C, Parks J, Wagner R, Kokjohn S, Reitz R. In-cylinder fuel blending of gasoline/diesel for improved efficiency and lowest possible emissions on a multi-cylinder light-duty diesel engine. SAE Technical Paper 2010-01-2206. https://doi.org/10.4271/2010-01-2206.
[8] Leermakers CAJ, van den Berge B, Luijten CCM, Somers LMT, de Goey LPH, Albrecht BA. Gasoline-diesel dual-fuel: effect of injection timing and fuel balance. SAE Technical Paper 2011-01-2437. https://doi.org/10.4271/2011-01-2437.
[9] Ickes A, Wallner T, Zhang Y, De Ojeda W. Impact of cetane number on combustion of a gasoline-diesel dual-fuel heavy-duty multi-cylinder engine. SAE Technical Paper 2014-01-1309. https://doi.org/10.4271/2014-01-1309.
[10] Heuser B, Ahling S, Kremer F, Pischinger S, Rohs H, Holderman B, Körfer T. Experimental investigation of a RCCI combustion concept with in-cylinder blending of gasoline and diesel in a light duty engine. SAE Technical Paper 2015-24-2452. https://doi.org/10.4271/2015-24-2452.
[11] Kokjohn S, Hanson R, Splitter D, Kaddatz J, Reitz R. Fuel reactivity controlled compression ignition in light- and heavy-duty engines. SAE Technical Paper 2011-01-0357. https://doi.org/10.4271/2011-01-0357.
[12] Pedrozo VB, May I, Guan W, Zhao H. High efficiency ethanol-diesel dual-fuel combustion: a comparison against conventional diesel combustion from low to full engine load. Fuel 2018;230:440–51. https://doi.org/10.1016/j.fuel.2018.05.034.
[13] Leermakers CAJ, Somers LMT, Johansson BH. Combustion phasing controllability with dual fuel injection timings. SAE Technical Paper 2012-01-1575. https://doi.org/10.4271/2012-01-1575.

[14] Ma S, Zheng Z, Liu H, Zhang Q, Yao M. Experimental investigation of the effects of diesel injection strategy on gasoline/diesel dual-fuel combustion. Appl Energ 2013; 109:202–12. https://doi.org/10.1016/j.apenergy.2013.04.012.
[15] Molina S, García A, Pastor JM, Belarte E, Balloul I. Operating range extension of RCCI combustion concept from low to full load in a heavy-duty engine. Appl Energ 2015;143:211–27. https://doi.org/10.1016/j.apenergy.2015.01.035.
[16] Ickes A, Hanson R, Wallner T. Impact of effective compression ratio on gasoline-diesel dual-fuel combustion in a heavy-duty engine using variable valve timing. SAE Technical Paper 2015-01-1796. https://doi.org/10.4271/2015-01-1796.
[17] Molina S, García A, Monsalve-Serrano J, Estepa D. Miller cycle for improved efficiency, load range and emissions in a heavy-duty engine running under reactivity controlled compression ignition combustion. Appl Therm Eng 2018;136: 161–8. https://doi.org/10.1016/j.applthermaleng.2018.02.106.
[18] Tuner M. Review and benchmarking of alternative fuels in conventional and advanced engine concepts with emphasis on efficiency, CO_2, and regulated emissions. SAE Technical Paper 2016-01-0882. https://doi.org/10.4271/2016-01-0882.
[19] Doosje E, Willems F, Baert R. Experimental demonstration of RCCI in heavy-duty engines using diesel and natural gas. SAE Technical Paper 2014-01-1318. https://doi.org/10.4271/2014-01-1318.
[20] Walker NR, Wissink ML, DelVescovo DA, Reitz RD. Natural gas for high load dual-fuel reactivity controlled compression ignition (RCCI) in heavy-duty engines. Proceedings of the ASME ICEF2014, paper ICEF2014-5620. doi: 10.1115/ICEF2014-5620.
[21] Splitter D, Hanson R, Kokjohn S, Reitz R. Reactivity controlled compression ignition (RCCI) heavy-duty engine operation at mid- and high-loads with conventional and alternative fuels. SAE Technical Paper 2011-01-0363. https://doi.org/10.4271/2011-01-0363.
[22] Splitter D, Wissink M, DelVoscovo D, Reitz R. RCCI engine operation towards 60% thermal efficiency. SAE Technical Paper 2013-01-0279. https://doi.org/10.4271/2013-01-0279.
[23] Curran S, Hanson R, Wagner R. Effect of E85 on RCCI performance and emissions on a multi-cylinder light-duty diesel engine. SAE Technical Paper 2012-01-0376. https://doi.org/10.4271/2012-01-0376.
[24] Benajes J, García A, Monsalve-Serrano J, Villalta D. Benefits of E85 versus gasoline as low reactivity fuel for an automotive diesel engine operating in reactivity controlled compression ignition combustion mode. Energ Conv Manag 2018;159: 85–95. https://doi.org/10.1016/j.enconman.2018.01.015.
[25] Cardona CA, Sánchez OJ. Fuel ethanol production: process design trends and integration opportunities. Bioresource Technol 2007;98:2415–57. https://doi.org/10.1016/j.biortech.2007.01.002.
[26] Joshi A. Review of vehicle engine efficiency and emissions. SAE Technical Paper 2019-01-0314. https://doi.org/10.4271/2019-01-0314.
[27] Mohr D, Shipp T, Lu X. The thermodynamic design, analysis and test of Cummins' Supertruck 2 50% brake thermal efficiency engine system. SAE Technical Paper 2019-01-0247. https://doi.org/10.4271/2019-01-0247.
[28] Benajes J, García A, Monsalve-Serrano J, Sari RL. Fuel consumption and engine-out emissions estimation of a light-duty engine running in dual-mode RCCI/CDC with different fuels and driving cycles. Energy 2018;157:19–30. https://doi.org/10.1016/j.energy.2018.05.144.
[29] Nieman DE, Morris AP, Neely GD, Matheaus AC, Miwa JT. Utilizing multiple combustion modes to increase efficiency and achieve full load dual-fuel operation in a heavy-duty engine. SAE Technical Paper 2019-01-1157. https://doi.org/10.4271/2019-01-1157.
[30] Li J, Yang WM, Goh TN, An H, Maghbouli A. Study of RCCI (reactivity controlled compression ignition) engine by means of statistical experimental design. Energy 2014;78:777–87. https://doi.org/10.1016/j.energy.2014.10.071.
[31] Box GEP, Wilson KB. On the experimental attainment of optimum conditions. J Roy Stat Soc B Met 1951;13:1–45.
[32] Pedrozo V, May I, Dallo Nora M, Cairns A, Zhao H. Experimental analysis of ethanol dual-fuel combustion in a heavy-duty diesel engine: an optimisation at low load. Appl Energ 2016;165:166–82. https://doi.org/10.1016/j.apenergy.2015.12.052.
[33] Spanjers CS, Beach CA, Jones AJ, Dauenhauer PJ. Increasing flame ionization detector (FID) sensitivity using post-column oxidation-methanation. Analytic Methods 2017;9:1928–34. https://doi.org/10.1039/c6ay03363f.
[34] Kar K, Cheng WK. Speciated engine-out organic gas emissions from a PFI-SI engine operating on ethanol/gasoline mixtures. SAE Technical Paper 2009-01-2673. https://doi.org/10.4271/2009-01-2673.
[35] Chang J, Güralp O, Filipi Z, Assanis D, Kuo T, Najt P, Rask R. New heat transfer correlation for an HCCI engine derived from measurements of instantaneous surface heat flux. SAE Technical Paper 2004-01-2996. https://doi.org/10.4271/2004-01-2996.
[36] Splitter D, Wissink M, DelVescovo D, Reitz R. Improving the understanding of intake charge effects for increasing RCCI engine efficiency. SAE Technical Paper 2014-01-1325. https://doi.org/10.4271/2014-01-1325.
[37] Egüz U, Maes NCJ, Leermakers CAJ, Somers LMT, de Goey LPH. Predicting auto-ignition characteristics of RCCI combustion using a multi-zone model. Int J Automot Techn 2013;14(5):693–9. https://doi.org/10.1007/s12239-013-0075-2.
[38] Kokjohn SL, Musculus MPB, Reitz RD. Evaluating temperature and fuel stratification for heat-release rate control in a reactivity-controlled compression-ignition engine using optical diagnostics and chemical kinetics modeling. Combust Flame 2015;162:2729–42. https://doi.org/10.1016/j.combustflame.2015.04.009.
[39] Sjoberg M, Dec J. Ethanol Autoignition Characteristics and HCCI Performance for Wide Ranges of Engine Speed, Load and Boost. SAE Int J Engines 2010;3(1): 84–106. https://doi.org/10.4271/2010-01-0338.
[40] Bekdemir C, Baert, R, Willems, F, Somers, B, Towards Control-Oriented Modeling of Natural Gas-Diesel RCCI Combustion, SAE Technical Paper 2015-01-1745, 2015, https://doi.org/10.4271/2015-01-1745.
[41] Musculus MPB, Kattke K. Entrainment waves in diesel jets. SAE Int J Engines 2009; 2:1170–93. https://doi.org/10.4271/2009-01-1355.
[42] Box GEP, Hunter JS, Hunter WG. Statistics for experimenters - design, innovation and discovery (2nd edition). Wiley; 2005.
[43] Olmeda P, García A, Monsalve-Serrano J, Sari RL. Experimental investigation on RCCI heat transfer in a light-duty diesel engine with different fuels: comparison versus conventional diesel combustion. Appl Therm Eng 2018;144:424–36. https://doi.org/10.1016/j.applthermaleng.2018.08.082.
[44] Willems RC, Willems FPT, Deen NG, Somers LMT. A Comparison of Low-Load Efficiency Optimization on a Heavy-Duty Engine Operated With Gasoline-Diesel RCCI and CDC. Proc ASME ICEF 2019. https://doi.org/10.1115/ICEF2019-7149.